Interferometric radar for activity recognition and benchmarking in different radar geometries

Boyu Zhou[1], Julien Le Kernec[2,3,4], Shufan Yang[3], Francesco Fioranelli[5], Olivier Romain[4], Zhiqin Zhao[2]

[1]Department of Computer Science, the University of Hong Kong, Hong Kong, China
[2] School of Information and Communication, University of Electronic Science and Technology of China, Chengdu, China
[3]James Watt School of Engineering, University of Glasgow, Glasgow, UK
[4]ETIS – Signal and Information Processing lab, University Cergy-Pontoise, Cergy, France
[5]MS3-Microwave Sensing Signals and Systems, TU Delft, Delft, The Netherlands
**Julien.lekernec@glasgow.ac.uk*

Keywords: CLASSIFICATION, HUMAN ACTIVITY RECOGNITION, HUMAN MICRO-DOPPLER, MACHINE LEARNING.

Abstract

Radar micro-Doppler signatures have been proposed for human activity classification for surveillance and ambient assisted living in healthcare-related applications. A known issue is the performance reduction when the target is moving tangentially to the line-of-sight of the radar. Multiple techniques have been proposed to address this, such as multistatic radar and to some extent, interferometric radar. A simulator is presented to generate synthetic data representative of 8 different radar systems (including configurations as monostatic, multistatic, and interferometric) to quantify classification performances as a function of aspect angles and deployment geometries. This simulator allows an unbiased performance evaluation of the different radar systems. 6 human activities are considered with signatures originating from motion-captured data of 14 different subjects. The results show that interferometric radar data with fusion outperforms the other methods with over 97.6% accuracy consistently across all aspect angles, as well as the potential for simplified indoor deployment.

1. Introduction

Radar signatures, in particular, micro-Doppler (mD) signatures (mDs), have attracted significant interests for human activity classification for security, healthcare, and assisted living applications [1].

An issue for classification based on mDs is the performance reduction for targets' trajectories tangential to the radar line of sight, as the mD frequency shifts are reduced, and it is challenging to extract informative features from the data. For example, Tahmoush [2] showed that micro-Doppler classification performance dropped to 40% at high aspect angles, and references [3-5] analysed the classification performance and limitations due to the aspect angle. When the target is not walking or moving along the radial direction, depending on the aspect angle, the salient features for classification may change, and the accuracy of classification reduces as the target velocity gets closer to the tangential direction.

As monostatic (MN) radar can only observe well the radial component of the mD signal, multiple cooperating radar sensors have been suggested to enhance the classification of mDs. This provides additional information from multistatic (MS) perspectives, at the price of increased system complexity to synchronize the different nodes [6, 7] separated by a baseline (the distance between nodes, e.g. transmitter (Tx) to receiver (Rx) in the bistatic case). An early implementation of simulated MS radar mDs from the Boulic model [8] for walk is presented in [9]. It shows how the fusion of the mDs of several nodes together may improve the quality and clarity of the mDs in comparison to only one node considering aspect angles at 0, 30 and 75° and different signal-to-noise ratios.

Interferometric (IFM) information has also been suggested as an alternative/complementary technique. Nanzer, in [10], presented an analysis of the angular velocity measurement of a person who is walking via a millimetre-wave correlation interferometer, which also covered the IFM measurement theory of angular velocity, and the frequency response simulations of a walking human participant.
The IFM channel provided information about the target angular velocity. This IFM signature is more pronounced as the baseline between the antennas is increasing. They showed that as the trajectory moved from a completely radial motion to completely tangential motion, the Doppler frequency shift decreased. In contrast, the IFM frequency shift increased for the walking action. Hence, these 2 detection modes can represent complementary measurements, improving the ability to measure the motion of randomly moving objects.

The research community has extensively focused on mDs for human radar classification. Still, this domain has shown limitations to distinguish between activities showing similar radial acceleration with respect to the radar, a.k.a. confusers. MS radar has been used to enhance classification accuracy with confusers and to tackle aspect angle issues, but the IFM sensing modalities has seldom been used in the literature.

In this paper, an IFM radar geometry is proposed that demonstrates robustness with respect to the aspect angle for indoor human activity recognition applications. The focus of this work is on generating synthetic mDs and, by association, IFM data. Several techniques have been used on mDs as it represents the majority of contributions on human activity recognition with radar to date. The classification techniques

include Bi-LSTM [11], LSTM [12], GRU [13], SAE, CAE [14], CNN [15], MFCC/FWCC [16] leading to increasingly better performances. A shallow CNN network (LeNet-5 [17]) has been selected here to perform the transfer learning from optical recognition to radar activity recognition in this work.

The paper is organized as follows. Section 2 describes the methodology to establish the simulation. Section 3 compares the results between the 8 radar systems. Finally, conclusions are given in Section 4.

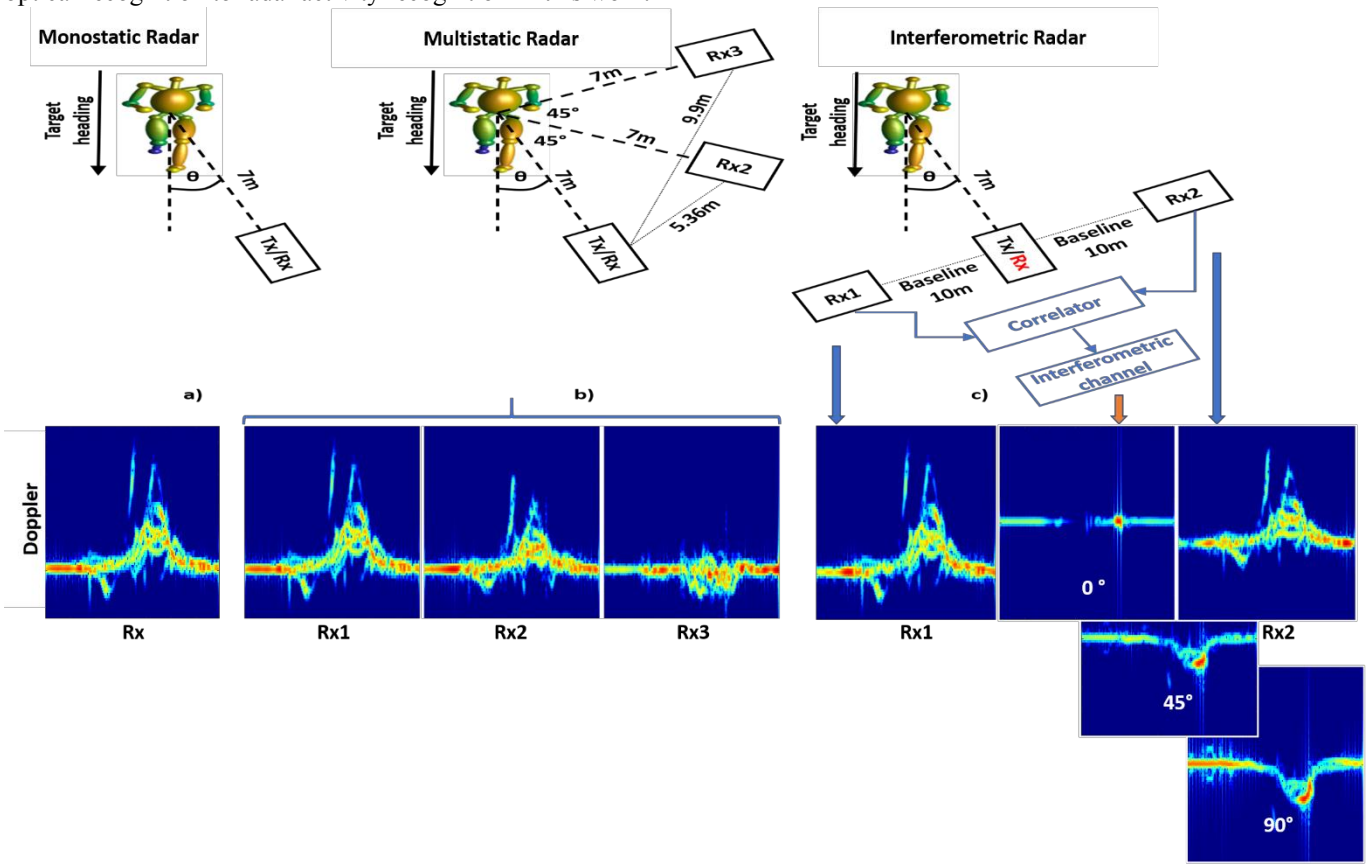

Fig. 1. *The simulation geometry for (a) MN radar system, (b) MS radar system - circular configuration with one transceiver and two bistatic receivers, and (c) IFM radar system (black and blue) & MS radar – in-line configuration (black and red).*

2. Methodology of the simulator

A framework to simulate and compare performances of 8 radar systems, was developed. This included a MN radar (Fig. 1a): relying on mDs from a single MN radar node; a MS radar (Fig. 1b): using 3 separate nodes, whose results are fused for classification purposes using majority voting; a MS radar (Fig. 1c black and red): using 3 separate nodes with baselines of 2, 5 & 10m, whose results are fused for classification purposes using a majority voting approacht; and finally an IFM radar (Fig. 1c black and blue): using 2 Rxs with baselines of 2, 5, & 10m, whose results are fused with the IFM channel for classification using majority voting.

Fig. 2 shows the Doppler shifts for a carrier at 9.8GHz for a target at 1m/s at the centre of the scene at varying aspect angles based on the theory in [7, 18]. The circular configuration was chosen at 0, 45, and 90° as it offered more diversity in Doppler shifts for a more robust classification compared to narrower bistatic angles with a Tx placement on the side as in [9]. The in-line configuration is inspired by [19]. Fig. 2a shows the most extensive variation in Doppler shifts with a 10m-baseline. As for the IFM channel, the configuration is based on [20].

The performance comparison is based on the accuracy of classification for 6 human motions where the aspect angle θ between the target heading and the radar line of sight changes from 0° to 90° with 5° per step in rotation. The details of the geometry of the different radar setups are shown in Fig. 1. It is important to note that the target may be translating, and the aspect angle does not remain constant. Instead, the heading of the target is considered to define the aspect angle.

The 6 classes of motions considered include (I) walking; (II) forward jumping; (III) kicking; (IV) sitting and standing; (V) running; (VI) walking on uneven terrain. These data originate from the Carnegie Mellon Motion capture (MoCap) database [15] or the HDM05 MoCap database [21]. Motion data in ASF/AMC format were used since this kind of skeleton-based data can comprise an explicit skeleton structure and also ensure that the bone lengths will be constant in the movement [15]. Motion data for head, torso, pelvis, legs, feet, arms, and hands were used to simulate radar returns.

The motion data was captured at 120 Hz in the database [15]. To simulate the Doppler frequency shift without aliasing, the sampling frequency was upsampled to 2 kHz before the simulation. The animation of human movement code was modified from [22], in particular, to generate MS and IFM signals and signatures.

Figure 3 shows a flow graph of the overall process for generation of synthetic radar signatures. For simplicity, the simulator assumed no free space losses, a noise-free environment, and no specific beam pattern. The total radar

return is a sum of backscattered signals from separate body parts. To get accurate radar returns, several parameters about the radar system should be set according to the specific scenarios, including the radar location, the bandwidth of the transmitted (Tx) signal (here equal to 400 MHz(, and the carrier frequency (here 9.8GHz). In simulating mDs, the ranges from the Tx/Rx to the target are represented by (1).

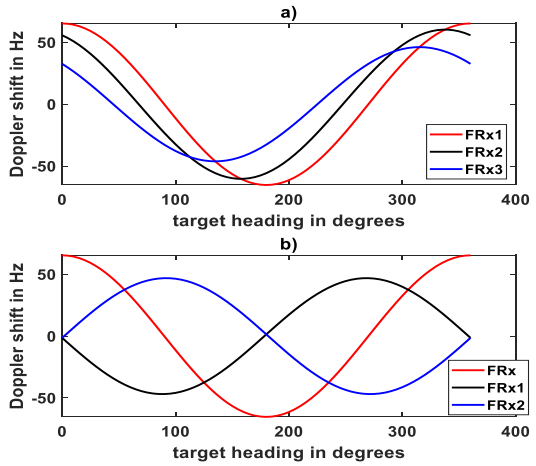

Fig. 2. *The expected Doppler shifts for a) the circular MS configuration with nodes at 0, 45, and 90°; b) the in-line configuration with a 10m baseline (Rx1/Rx2 have the same Doppler shifts in the IFM case) for a carrier frequency of 9.8GHz.*

$$r_T = r_t + vt, \quad r_R = r_r + vt \tag{1}$$

r_t and r_r denote the initial ranges from the Tx antenna and the Rx antenna to the target respectively; r_T and r_R denote the ranges as a function of time t; v denotes the relative radial velocity of the moving object to the radar. The total phase change between the Tx signal and the scattered signal is proportional to the total length of propagation, which can be calculated by (2).

$$\Delta\phi = 2\pi \frac{r_T + r_R}{\lambda_c} \tag{2}$$

where $\lambda_c = c/f_c$ denotes the Tx signal wavelength, c denotes the speed of light in m/s, and f_c is the carrier frequency. When the Tx and the Rx are static, the Doppler shift f_d can be calculated by (3).

$$f_d = \frac{1}{2\pi}\frac{d}{dt}\Delta\phi = \frac{2v}{\lambda_c} \tag{3}$$

where the observed frequency is proportional to the relative radial velocity. The complex Doppler signal at the Rx can be represented by (4)

$$S(t) = Ae^{-j2\pi f_c\left(\frac{2r(t)}{c}\right)} \tag{4}$$

where A denotes the radar cross-section (RCS), f_c is the frequency of the Tx signal, and $r(t)$ denotes the distance from the radar to the target [22].

The simulation represents the 2 received (Rx) signals of the IFM radar system by (5).

$$S_1(t) = A_1 e^{j2\pi f_r t}, S_2(t) = A_2 e^{j2\pi f_r (t-\tau)} \tag{5}$$

where τ denotes the time delay of signal reception between the 2 Rx signals [23], A_1& A_2 denote the target RCS viewed from Rx 1 & 2, and f_r is the Rx frequency. For the IFM measurement, the time delay can be calculated by (6).

$$\tau = \frac{D}{c}\sin(\theta) = \frac{D}{c}\sin(\omega t) \tag{6}$$

where ω is the angular velocity of the target, θ denotes the angle off the broadside, D is the baseline between the 2 Rxs, and c is the speed of the electromagnetic signal. The IFM response after correlator is the product and integration of the 2 Rx signals as shown in (7) [23].

$$S_i(t) = A_1 A_2 e^{j2\pi f_r \tau} = A_1 A_2 e^{j2\pi f_r \frac{D}{c}\sin(\omega t)} \tag{7}$$

where f_r is the frequency of the Rx signal.

The observed IFM frequency can be calculated by (8).

$$f_s = \frac{d}{dt} f_r \frac{D}{c}\sin(\omega t) = f_r \frac{\omega D}{c}\cos(\theta) \tag{8}$$

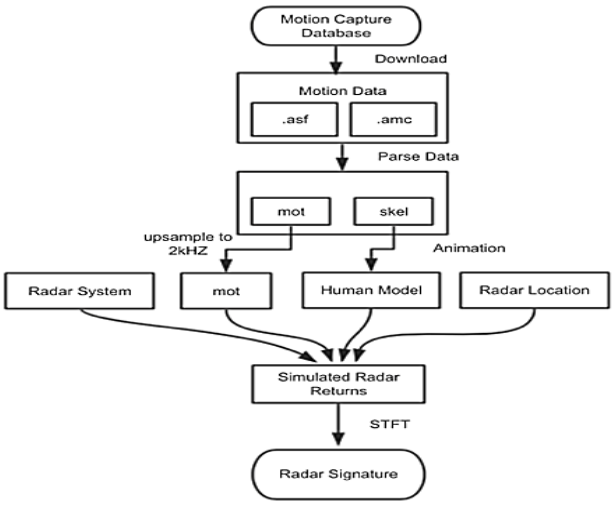

Fig. 3. *Flow graph of the radar signature simulator algorithm based on motion-captured data*

In the simulation, the value of the RCS is used as the amplitude of the complex response signal. If the Rx and the Tx are not located at the same place, the RCS should be calculated by its bistatic expression. The resulting IFM and Doppler responses are both processed in the time-frequency domain using Short Time Fourier Transform (STFT). The STFT separates the time-varying signal into shorter segments using overlapped Gaussian windows with a length of 256 samples (128 ms at 2 kHz pulse repetition period) and processes each data window using Fourier transform to calculate the frequency components.

A total of 88 different motion files performed by 14 subjects from CMU database were simulated to generate the training/testing datasets. These were used to generate the frequency responses at different aspect angles. It was not possible to have all 6 actions all the time from the same subject due to the limitations of this dataset. Samples from every trial data were divided as 1-second long snapshots to increase the size of the dataset. Every class has 80 samples, thus 480 in total. 360 samples (75%) are chosen as the training data, and the classification algorithm will test the other 120 samples (25%) in every scenario (Table 1). The test samples for different classification methods were simulated from the same motion data files to ensure a fair comparison.

Convolutional Neural Networks (CNNs) use mDs as input for classification and extract features automatically. The MN radar relies on one mDs, processed by a single CNN. The IFM

radar system implemented majority voting [24] as a decision-level fusion mechanism on the output labels from 2 mDs, and one IFM frequency response. Therefore, it needed 3 separate CNNs. The MS radar system also utilized the same fusion mechanism from 3 mDs from different radar nodes, hence it also needed 3 CNNs. In total, in every tested scenario, one CNN was trained per channel using the corresponding frequency responses and mDs.

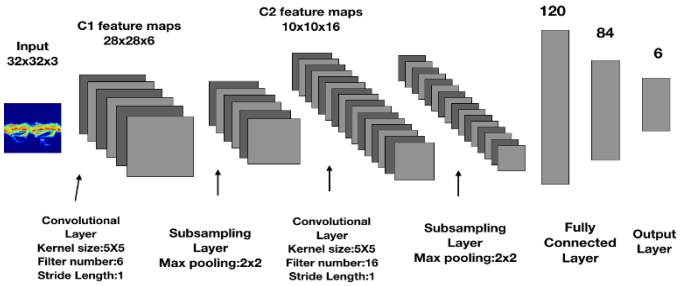

Fig. 4. *Structure of CNN used in this article as a classifier*

Table 1 Summary of motion data samples from CMU

Actions	Number of subjects	Number of files	Training set	Testing set
I walking	3(subject 02,07,08)	18	60	20
II forward jumping	5(subject 13,16,83,91,105)	23	60	20
III kicking	1 (subject 144)	4	60	20
IV sitting and standing	2 (subject 13,13)	9	60	20
V running	2 (subject 09,35)	21	60	20
VI walking on uneven terrain	1 (subject 36)	13	60	20

Table 2 Hyperparameters for CNN

Hyperparameters	**Value**
Learning rate	0.012~0.013
Mini Batch size	24
L2 Regularization ratio	0.0005
Dropout rate	0.5
Solver	Stochastic Gradient Descent
Momentum	0.9
MiniBatchSize	16
Max Epochs	150

The network architecture modified from LeNet-5 [17] (Fig. 4), was adopted for all of CNNs with only small differences in the hyperparameters, as given in Table 2.

Summarising, the signatures are generated by an accurate simulation of human motion based on motion-captured data from live volunteers [15]. Thus, the kinematics reflect natural movements. The signatures are based on proven simulation methods from [22], which is then extended using analytical equations for RCS in MN and bistatic configurations from [25]. Lastly, the theoretical frameworks for the bistatic and IFM channels were demonstrated in [7, 10, 20, 23].

3. Results and discussions

3.1. mD and IFM responses examples

For all 8 radar systems, the signatures for each of the Rxs were captured from 0° to 90° with 5° steps in rotation. This section comments on some examples of the signatures to visualize the phenomenology better. Fig. 1 showed the mDs of the transceiver node from the circular MS radar system at 3 aspect angles 0°, 45°, and 90°. It can be observed from the mDs that the Doppler spread and mean decrease as the aspect angle in rotation increases from 0° to 90°. At 90°, the action is barely distinguishable.

Fig. 1 also depicted the IFM response obtained at different aspect angles for a fixed baseline of 10m. The IFM channel increases in amplitude as the aspect angle increases from 0° to 90°. Furthermore, the greater the baseline, the larger the amplitude registered is expected to be, as the aspect angle increases.

Note, that there are spikes in the responses; those are simulation artefacts caused by the processing by segments known as edge effects [22], and they occur at the junction between 2 segments of processed data.

3.2. Comparison of different radar systems

These 8 radar geometries were compared in classification accuracy for the scenarios where the aspect angle changes from 0° to 90° with 5° steps. In every chosen aspect angle, every network associated with each radar channel was repeatedly trained ten times through a cross-validation process, and then their decisions were fused. The final accuracy, as shown in Fig. 5, is based on the average classification results for MN (1 network), circular and in-line MS (3 networks and decision-level fusion), and IFM (3 networks and decision-level fusion) configurations.

The MS radar (in-line or circular) performs best from 0° to 35° with up to 1.15% improvement in accuracy. However past 35°, the performances of the circular MS radar drop under the performance of the IFM and in-line MS systems. The method relying only on the single mD signature from the MN radar system shows a downward trend in the performance, and it degrades severely where the aspect angle is larger than 65°, as expected. The average accuracy is only 80.92% at 90°. Although the circular MS radar performs better than MN, its accuracy drops under 95% after 45° and even lower between 80 to 90° aspect angles. It can be observed that the IFM radar maintains over 97.58% accuracy for all aspect angles ranging from 0° to 90°, whereas the in-line MS maintains 94% accuracy. The in-line maintains consistent performances up to 60° with the IFM radar. The IFM radar accuracy improves by +2.4% at 45° to +16.6% at 90° compared to MN radar. The accuracy up to 40° is comparable for the MS and IFM systems. The IFM system outperforms the in-line MS radar for larger aspect angles between 75 and 90°.

To further investigate the robustness of the proposed methods, the baseline between the Txs and the Rxs of the IFM radar was also set to 2 and 5 m, respectively. The classification results are shown in Fig. 5. The radar system with a 5 m baseline has similar performances with the 10 m baseline, with only a minor performance degradation ranging from [0.1 to 1.5%] for the IFM radar. The average accuracy with a 5 m baseline in every scenario fluctuates around 98%, and its minimum value is 97.08%. Below 55° aspect angle, the IFM radar with a 2m baseline performs similarly to the 10m baseline radar, but the performances decline to 91.58% at 90°. Additionally, the 2m-baseline IFM system has better performances than the MN, 2m-baseline in-line MS, and circular MS radar systems. The in-line IFM radar system, however, is not performing well with a reduction in the baseline with performances dropping severely after 55° to 94% and ~91% at 90° with 5m baseline. Furthermore, the stability,

up to 55° worsens and fluctuates between 97 and 99%. The degradations are worse with 2m baseline.

4. Conclusion

In this paper, 8 radar systems, namely MN, MS (circular & in-line), and IFM for 6 classes of motions were simulated and compared in scenarios where the aspect angle to the target changes from 0° to 90°. A total of 88 different motion data files performed by 14 human subjects from CMU were simulated to generate corresponding mDs and corresponding interferograms. In every scenario, one CNN was trained per channel to perform the tasks of classification and comparison. From the simulation results given in Section 3, the IFM radar with suitable baseline and fusion of the mD signatures and the IFM frequency responses has more consistent capabilities over the other systems to discriminate between the different activities, throughout the whole range 0° to 90° in aspect angle. The joint use of IFM frequency response and mD signatures yield an accuracy of over 97.58% in all scenarios with a 10m baseline and 97.08% with 5m. Even with a reduction in the baseline, the IFM radar maintains good performances.

In contrast, the performance degradation for the in-line MS radar would not be acceptable for operational deployment considering indoor applications. Additionally, for the IFM radar, the higher the carrier frequency, the smaller the baseline has to be to benefit from the same performances. With the advent of millimetre-wave technologies, a similar level of performances will be available with a much smaller form factor for indoor scenarios, whereas in-line MS radar would require a significant baseline to maintain good performances and may not be suitable for indoor environments.

Future work will look at feature level fusion for the implementation of classification to reduce the computational load, and lightweight implementation of the networks to reduce their size and time for training and inference.

Acknowledgment

The authors would like to thank the British Council 515095884 and Campus France 44764WK – PHC Alliance France-UK for their financial support.

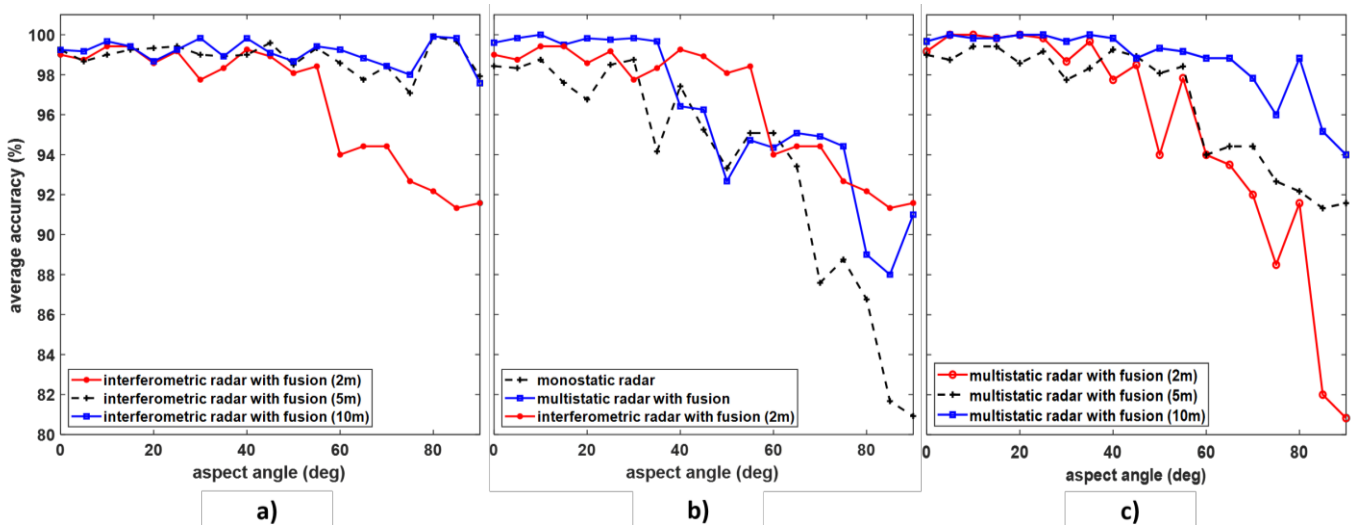

Fig. 5. *Comparison of results a) Classification results of IFM radar systems with 2m, 5m, 10m baseline respectively; b) comparison of IFM radar with 2m baseline with MN and MS radar (circular); c) comparison of MS radar (in-line) with 2m,5m and 10m baseline .*

References

[1] J. L. Kernec *et al.*, "Radar Signal Processing for Sensing in Assisted Living: The challenges associated with real-time implementation of emerging algorithms," *IEEE Signal Processing Magazine,* vol. 36, no. 4, pp. 29-41, 2019, doi: 10.1109/MSP.2019.2903715.

[2] D. Tahmoush and J. Silvious, "Radar micro-doppler for long range front-view gait recognition," in *2009 IEEE 3rd International Conference on Biometrics: Theory, Applications, and Systems*, 28-30 Sept. 2009 2009, pp. 1-6, doi: 10.1109/BTAS.2009.5339049.

[3] B. Tekeli, S. Z. Gurbuz, and M. Yuksel, "Information-Theoretic Feature Selection for Human Micro-Doppler Signature Classification," *IEEE Transactions on Geoscience and Remote Sensing,* vol. 54, no. 5, pp. 2749-2762, 2016, doi: 10.1109/TGRS.2015.2505409.

[4] S. Z. Gürbüz, B. Erol, B. Çağlıyan, and B. Tekeli, "Operational assessment and adaptive selection of micro-Doppler features," *IET Radar, Sonar & Navigation,* vol. 9, no. 9, pp. 1196-1204, 2015, doi: 10.1049/iet-rsn.2015.0144.

[5] Y. Kim and H. Ling, "Human Activity Classification Based on Micro-Doppler Signatures Using a Support Vector Machine," *IEEE Transactions on Geoscience and Remote Sensing,* vol. 47, no. 5, pp. 1328-1337, 2009, doi: 10.1109/TGRS.2009.2012849.

[6] F. Fioranelli, M. Ritchie, and H. Griffiths, "Centroid features for classification of armed/unarmed multiple personnel using multistatic human micro-Doppler," *IET Radar, Sonar & Navigation,* vol. 10, no. 9, pp. 1702-1710, 2016.

[7] N. J. Willis, *Bistatic radar*. Scitech publishing Inc., 2005.

[8] R. Boulic, N. M. Thalmann, and D. Thalmann, "A global human walking model with real-time kinematic personification," *The Visual Computer,* vol. 6, no. 6, pp. 344-358, 1990/11/01 1990, doi: 10.1007/bf01901021.

[9] C. Karabacak, S. Z. Gürbüz, and A. C. Gürbüz, "Radar simulation of human micro-Doppler signature from video motion capture data," in *2013 21st Signal Processing and Communications Applications Conference (SIU)*, 24-26 April 2013 2013, pp. 1-4, doi: 10.1109/SIU.2013.6531365.

[10] J. A. Nanzer, *Interferometric measurement of the angular velocity of moving humans* (SPIE Defense, Security, and Sensing). SPIE, 2012.

[11] H. Li, A. Shrestha, H. Heidari, J. L. Kernec, and F. Fioranelli, "Bi-LSTM Network for Multimodal Continuous Human Activity Recognition and Fall Detection," *IEEE Sensors Journal,* pp. 1-1, 2019, doi: 10.1109/JSEN.2019.2946095.

[12] S. Yang, J. L. Kernec, F. Fioranelli, and O. Romain, "Human Activities Classification in a Complex Space Using Raw Radar Data," presented at the International Radar Conference, Toulon, France, 23-27 Sept, 2019.

[13] M. Wang, G. Cui, X. Yang, and L. Kong, "Human body and limb motion recognition via stacked gated recurrent units network," *IET Radar, Sonar & Navigation,* vol. 12, no. 9, pp. 1046-1051, 2018, doi: 10.1049/iet-rsn.2018.5054.

[14] S. Z. Gurbuz and M. G. Amin, "Radar-Based Human-Motion Recognition With Deep Learning: Promising applications for indoor monitoring," *IEEE Signal Processing Magazine,* vol. 36, no. 4, pp. 16-28, 2019, doi: 10.1109/MSP.2018.2890128.

[15] Y. Lin, J. L. Kernec, S. Yang, F. Fioranelli, O. Romain, and Z. Zhao, "Human Activity Classification With Radar: Optimization and Noise Robustness With Iterative Convolutional Neural Networks Followed With Random Forests," *IEEE Sensors Journal,* vol. 18, no. 23, pp. 9669-9681, 2018, doi: 10.1109/JSEN.2018.2872849.

[16] M. S. Seyfioglu, B. Erol, S. Z. Gurbuz, and M. G. Amin, "DNN Transfer Learning From Diversified Micro-Doppler for Motion Classification," *IEEE Transactions on Aerospace and Electronic Systems,* vol. 55, no. 5, pp. 2164-2180, 2019, doi: 10.1109/TAES.2018.2883847.

[17] Y. Lecun, L. Bottou, Y. Bengio, and P. Haffner, "Gradient-based learning applied to document recognition," *Proceedings of the IEEE,* vol. 86, no. 11, pp. 2278-2324, 1998, doi: 10.1109/5.726791.

[18] F. Fioranelli, M. Ritchie, and H. Griffiths, "Aspect angle dependence and multistatic data fusion for micro-Doppler classification of armed/unarmed personnel," *IET Radar, Sonar & Navigation,* vol. 9, no. 9, pp. 1231-1239, 2015, doi: 10.1049/iet-rsn.2015.0058.

[19] Z. Chen, G. Li, F. Fioranelli, and H. Griffiths, "Personnel Recognition and Gait Classification Based on Multistatic Micro-Doppler Signatures Using Deep Convolutional Neural Networks," *IEEE Geosci. Remote Sens. Lett.,* vol. 15, no. 5, pp. 669-673, 2018, doi: 10.1109/LGRS.2018.2806940.

[20] J. A. Nanzer, "Micro-motion signatures in radar angular velocity measurements," in *2016 IEEE Radar Conference (RadarConf)*, 2-6 May 2016 2016, pp. 1-4, doi: 10.1109/RADAR.2016.7485234.

[21] M. Muller, T. Roder, M. Clausen, B. Eberhardt, B. Kruger, and A. Weber, "Documentation Mocap Database HDM05," Institut fur informatik II Universitat Bonn D-53117 Bonn, Germany, CG-2007-2, 2007 2007.

[22] V. Chen, *The Micro-Doppler Effect in Radar*. London, Boston: Artech House, 2011.

[23] J. A. Nanzer and V. C. Chen, "Microwave interferometric and Doppler radar measurements of a UAV," in *2017 IEEE Radar Conference (RadarConf)*, 8-12 May 2017 2017, pp. 1628-1633, doi: 10.1109/RADAR.2017.7944468.

[24] H. Li, A. Shrestha, H. Heidari, J. Le Kernec, and F. Fioranelli, "A Multisensory Approach for Remote Health Monitoring of Older People," *IEEE J. of Electromagn., RF and Microw. in Med. and Biol.,* vol. 2, no. 2, pp. 102-108, 2018, doi: 10.1109/JERM.2018.2827099.

[25] K. D. Trott, "Stationary Phase Derivation for RCS of an Ellipsoid," *IEEE Antennas and Wireless Propagation Letters,* vol. 6, pp. 240-243, 2007, doi: 10.1109/LAWP.2007.891521.